RSC Advances

PAPER

View Article Online
View Journal | View Issue

Cite this: *RSC Adv.*, 2022, **12**, 28059

Non-wettable/wettable coatings floating on liquid metal marbles for anti-combination, reversible conductivity transformation and magnetic motion in solution†

Junfeng Zhao,[a] Xu Bi[ab] and Han Dai *[ab]

Received 28th July 2022
Accepted 27th September 2022

DOI: 10.1039/d2ra04706c

rsc.li/rsc-advances

Novel non-wetted/wetted floatable polyethylene/Cu and porous-Ni/Cu (P–Ni/Cu) coatings have been designed and fabricated for anti-combination of gallium-based liquid metal alloy (LM) marbles in solutions. Both coated LM pairs show strong anti-combination resistances even under a large extrusion ratio. Additionally, both coatings also show strong bonding forces with LMs and are floatable on the surfaces of LMs. Driven by electric or magnetic fields, floatable polyethylene/Cu or P–Ni/Cu coatings on LM surfaces are guided by these external fields, and then restore the original arrangement by the surface tension of the LMs and buoyancy of the coatings themselves after removing external fields, by which these coated LM marble or LM marble pair exhibit the revisable conductivity transitions and magnetic driven motion applications. This work should present a new way for the clustering and functional application of LMs in solutions.

Introduction

In recent years, gallium-based room temperature liquid-metal alloys (LMs), such as EGaIn and GaInSn have been stimulating great enthusiasm for research in chip cooling, floating electrodes and robotics due to their high thermal/electrical conductivity and large-scale changeable surface tension.[1–4] Many studies on gallium-based room temperature LM robots (generally LM marbles due to their high surface tension) are carried out in acidic or alkaline environments, mainly because of the regulation of the naturally formed oxide films on their surfaces and/or the convenience of applying electric fields.[5] However, once the oxide layer on the surface of the LM marbles is removed by the acidic or alkaline environment or destroyed by mechanical force, the metal surface appears as an atomically smooth mirror. And when these LM marbles approach each other, they will combine together rapidly.[6] Owing to this, only one LM marble is commonly allowed in a free space for the robotic application, which obviously severely restricts their cluster development.

The organic coating method is very effective and widely used to avoid agglomeration of nano-scale gallium-based LMs particles.[7] However, at the macro-scale, micron-thick organic coatings generally make LM marbles become insulators.[8] Although highly conductive coatings like graphene can effectively improve the conductivity of LM marbles, these organic or graphene coatings will fall off the surface of LM marbles rapidly when they are submerged in the acid or alkaline solutions due to the dissolution of the viscous oxide layer on LM marbles.[9] As a result, both the conductivity and the bonding stability to LMs of the anti-combination coatings should also be considered in the solution.

As reported, Cu, Ag, Ge *et al.* can be highly wetted by gallium-based LMs in acid or alkaline solutions.[10,11] Especially, Cu can easily react with liquid Ga as $CuGa_2$, which greatly enhances the bonding between Cu and LM alloys.[12–14] However, as reported, such intermetallic wetting between Cu, Ag and gallium-based LMs will inevitably cause irreversible internalization,[15] which strictly limits their usage as coating materials for LMs.

Inspired from amphiphilic molecules used in ordinary detergent, herein novel polyethylene/Cu and porous Ni/Cu non-wettable/wettable structures have been designed and fabricated for anti-combination of the gallium-based LM marbles in solutions. The inner Cu layer (wettable) provides bonding forces with the LMs, while the outer layer of polyethylene (non-wettable) is to achieve the anti-combination function. It is found that both pairs of LMs with polyethylene/Cu or P–Ni/Cu coatings show good anti-combination properties even at a large extrusion ratio. What's more, LM marbles coated with polyethylene/Cu or P–Ni/Cu also realized other functions, such as reversible conductivity transformation and motion driven by electric or magnetic fields, due to their highly floatable

[a]*Laboratory of Advanced Light Alloy Materials and Devices, Yantai Nanshan University, Longkou 265713, China. E-mail: daihan1985@189.cn*

[b]*Yulong Petrochemical Co., Ltd., Longkou 265700, China*

† Electronic supplementary information (ESI) available. See https://doi.org/10.1039/d2ra04706c

properties. Owing to the reasons above, this work realizes the anti-combination of the gallium-based LM marbles in solution and shows great potential applications in various gallium-based LM devices by changing the appropriate functional outer layers.

Experimental

Gallium-based LM alloys were prepared by mixing Ga 67.0 wt%, In 20.5wt%, Sn 12.5wt% with purity of 99.9%, in a water bath at 50 °C for complete fusing; the melting temperature of the LM alloys is around 10 °C. Pure Cu foil (thickness 0.05 mm), Porous Ni (P–Ni) (thickness 0.1 mm, average porous 0.1 mm) and polyethylene (thickness 0.025 mm) were cut into round pieces with a diameter of 0.1 cm (Cu, P–Ni), 0.2 cm (Cu, P–Ni), 0.3 cm (Cu, P–Ni), 0.5 cm (polyethylene), and 0.7 cm (polyethylene) respectively. Then these pieces were washed with ethanol in a sonication bath for 3 min and dried naturally. And then, a phenolic resin modified neoprene adhesive is used to stick Cu layers at the center of P–Ni and polyethylene layers. Rubidium magnets and a DC power supply have been used to drive coated LMs marbles. The micro-morphologies of the surface of polyethylene, Cu and P–Ni were measured by optical microscope (Zeiss, LX-047PBT). The thermal conductivity of LMs, and LM coated polyethylene/Cu coatings is measured by Metter Toledo 1/700 Differential Scanning in air rather than in HCl solution. Other optical photos and video data of the phenomenon were shot by a Huawei nova7 mobile phone.

Results and discussion

The non-wettable/wettable coatings are presented in Fig. 1(a). The inner Cu layer (wettable) provides the bonding force with the LMs, while the outer polyethylene or P–Ni layer (non-wettable) is to achieve some specific functions, especially anti-combination function. Polyethylene-Cu coating designs are asymmetric, with the diameter of polyethylene layer much larger than that of Cu to obtain better anti-combination abilities. On the contrary, the coating designs for the P–Ni layer are symmetrical on both sides to enhance their flexibility. Optical images of polyethylene/Cu, P–Ni/Cu and the surface morphologies of Cu, polyethylene and P–Ni are presented in Fig. 1(b) and (c). Inset images in Fig. 1(b) and (c) show the wettability of LMs to Cu (wetting angle 46.3°), polyethylene (wetting angle 117.5°) and P–Ni (wetting angle 121.5°). After these coatings are submerged in HCl solution (0.4 mol L^{-1}), the inner Cu layer easily becomes bonded to and floats on the surface of gallium-based LM marbles to resist their combination (Fig. 1(d) and (e)).

Fig. 2 shows the combination resistance of polyethylene/Cu, P–Ni/Cu coatings with various diameters. A scheme and two optical images of combination resistance tests of LMs marble pairs with polyethylene/Cu, P–Ni/Cu coatings are presented in Fig. 2(a)–(c). The compression rate here is kept at about 1 mm s^{-1} for each test. The maximum compression sets before the combination of coated LMs marble pairs are presented in Fig. 2(d). For polyethylene/Cu coatings with a diameter of 0.3 cm/0.2 cm, the LMs marble pairs can tolerate nearly 20% extrusion ratio without combination. Since combination resistance is mainly due to physical isolation caused by external polyethylene layers, stronger combination resistance is obtained by polyethylene layers with larger diameters, for they have more redundant area to protect the marbles. Comparatively, the whole combination resistance of P–Ni/Cu coatings is stronger (with a minimum tolerance of nearly 40% deformation). P–Ni/Cu coatings feature in the electrochemical reaction enhanced combination resistance in HCl solution instead of physical isolation of polyethylene/Cu coatings. It is well known that the standard electrode potential of Ga (−0.55 V), being reduced after alloying with In and Sn, is much lower than that of Ni (−0.25 V) and Cu (0.34 V).[16,17] Hydrogen bubbles generated by the electrochemical reactions (Fig. 1(e) and 2(c)) will converge on and surround the P–Ni/Cu coatings, and hence inhibiting the combination of LMs marbles. P–Ni/Cu coatings with smaller diameters generate more uniform bubbles and bring stronger combination resistance. Above all, both polyethylene/Cu and P–Ni/Cu coatings show strong combination resistance for LMs marble pairs in solution.

Obviously, the strength of the bonding force between coatings and LMs is another important parameter for their quality evaluation. A lifting device as shown in Fig. 3(a) has been used to measure the bonding force between coatings and LMs through recording the maximum lifting forces. Herein, only the

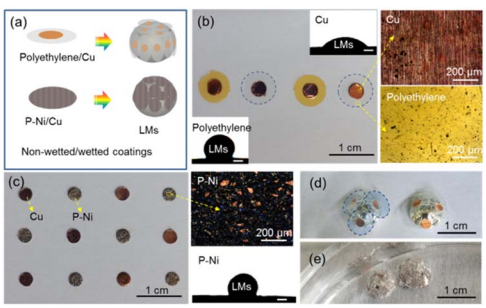

Fig. 1 (a) Scheme of the polyethylene/Cu and P–Ni/Cu non-wettable/wettable coatings on LM marbles; (b) and (c) Optical images of polyethylene/Cu, P–Ni/Cu and the surface morphologies of Cu, polyethylene and P–Ni; inset images are the wetting angle tests of LMs on Cu, polyethylene and P–Ni surfaces; the scale bars of the wetting angle tests are 1 mm. (d) and (e) LMs marbles with polyethylene/Cu and P–Ni/Cu coatings on them.

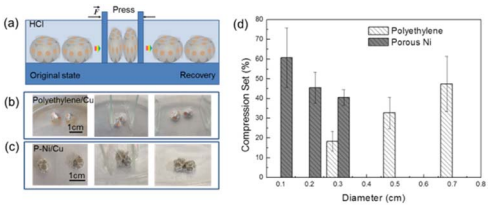

Fig. 2 (a)–(c) Scheme and optical images of the combination resistance tests of LMs marbles coated with polyethylene/Cu and P–Ni/Cu; (d) Combination resistance tests of polyethylene/Cu (diameters 0.3 cm/0.2 cm, 0.5 cm/0.3 cm, 0.7 cm/0.3 cm) and P–Ni/Cu (diameters 0.1 cm/0.1 cm, 0.2 cm/0.2 cm, 0.3 cm/0.3 cm) coated LMs marbles.

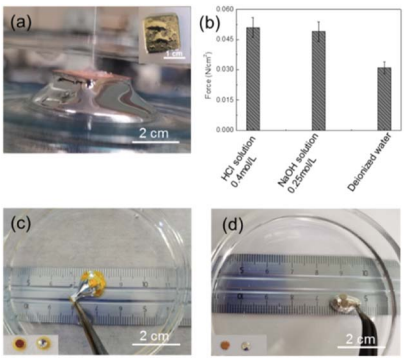

Fig. 3 (a) Lifting device for the tests of the bonding force of coatings in solution, inset image is the Cu surface adhered on LMs the after the vertical lifting; (b) bonding force between Cu and LMs per-unit area in HCl, NaOH and deionized water; (c) and (d) vertical pull of the polyethylene/Cu and P–Ni/Cu coatings out of the surface of LMs marbles, inset images are the coatings adhered on LMs before and after the vertical lifting.

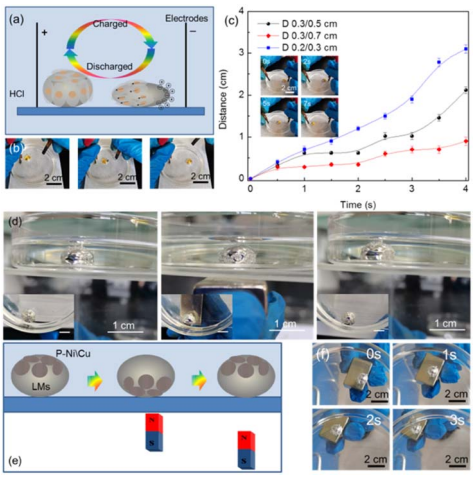

Fig. 4 (a) and (b) Scheme and optical images of electric field/surface tension & buoyancy driven reversible shifts of polyethylene/Cu coatings; (c) electric field driven movements of LMs marbles coated with polyethylene/Cu of various diameters; (d) and (e) optical images and scheme of magnetic field/surface tension & buoyancy driven reversible shifts of P–Ni/Cu coatings; (f) magnetic field driven movements of LMs marbles coated with P–Ni/Cu with 0.3 cm/0.3 cm diameters.

bonding force of polyethylene/Cu has been presented in Fig. 3(b) due to the same bonding layer of P–Ni/Cu coatings. It can be clearly observed that the maximum lifting forces between polyethylene/Cu coatings with LMs are similar (about 0.05 N cm^{-2}) in hydrochloric acid or NaOH solutions, but become lower in deionized water (around 0.03 N cm^{-2}), which are calculated by the ratio of measured tensions F and contact area S of the coatings. The possible reason is that the bonding force between coatings and LMs is much higher than the surface tension of LMs. Through the lifting, the measured maximum forces are originally from the surface tension of LMs, and thus showing similar values no matter in hydrochloric acid or NaOH solutions. When LMs are submerged in deionized water, the instantaneously formed oxide layer will significantly reduce the surface tension of LMs, and then the maximum lifting forces will be greatly reduced accordingly. Furthermore, the serious deformation of LMs marbles, induced by the direct and vertical pulling of the polyethylene/Cu and P–Ni/Cu coatings and the LMs fully adhered to Cu surfaces (inset in Fig. 3(a), (c) and (d)), further proves the strong bonding force between coatings and LMs. Apparently, the high bonding force between the polyethylene/Cu, P–Ni/Cu and LMs is beneficial for its coating application in solution.

As above, the strong bonding force between the non-wettable/wettable coatings and LMs mainly originates from the surface tension of LMs. Owing to this, the bonding of these non-wettable/wettable coatings should be very small in the tangential direction, which makes the shifts of these coatings on the surface of LMs fairly easy. In other words, the non-wettable/wettable coatings can be considered as floating on the surface of LMs. Fig. 4(a) and (b) show that the polyethylene/Cu coatings are pushed opposite to the moving direction of LMs marbles by the 4 V electric field induced surface flow.[18] When the electric field is removed, the polyethylene/Cu coatings are quickly restored to the cover of LMs marble by the surface tension of LMs and their own buoyancy. Because the polyethylene/Cu coatings are non-conductive, such reversible shifts of polyethylene/Cu coatings are expected to realize the electric field induced switching of the circuit in solution (Fig. S1†). In addition, the thermal conductivity of LMs changes from about 15 ± 5 W m^{-1} K to 30 ± 10 W m^{-1} K during the close/open of polyethylene/Cu coatings, which also shows their potential usage as changeable thermal conductivity materials. Apparently, the function above requires larger polyethylene/Cu coatings to obtain better performance. However, the electric field induced motion tests show that polyethylene/Cu coatings with larger diameters exhibit greater motion resistance, as shown in Fig. 4(c). Therefore, it is necessary to balance the motion abilities with the improvement of other functions of LMs. As shown in Fig. 4(d) and (e), the reversible shifts of P–Ni coatings on the surface of LMs marbles can be driven similarly by magnetic field and can be restored by the surface tension of LMs and buoyancy of porous Ni when the magnetic field is removed. The difference between the two is that, in the electric field, the coatings are driven to move by the LMs marbles, while in magnetic field (Fig. S2†), the LMs marbles are driven to move by the coatings. What's more, both coatings show high durability (Fig. S3†), which guaranteed their usage in the solutions. Above all, such non-wettable/wettable and floatable coating design concept provides a new design strategy for the functional applications of LMs marble based devices.

Apparently, this non-wetted/wetted floatable coating design efficiently avoids the combination between LMs marbles. And the functional outer layers realize the reversible conductivity transformation and magnetic motion of LMs marbles. In addition, from the perspective of the functional properties of the surface of LMs marbles themselves, such as the platinum catalysis,[19] the interfacial bismuth precipitation on the surface of LMs,[20] such eclectic or magnetic field induced reversible spreading and closing of the coatings should be beneficial for

their processes control and protect internal functional materials in the non-working state.

Conclusions

In summary, we reported novel non-wettable/wettable and floatable polyethylene/Cu and P–Ni/Cu coatings for anti-combination of LMs marbles. Both coatings have strong resistance to combination of LM marbles. For the polyethylene/Cu coatings, physical isolation is the main source for the resistance to combination, so the larger the polyethylene diameter, the stronger the anti-combination abilities. For polyethylene/Cu coatings, the LM marble pairs show a minimum tolerance of nearly 20% extrusion ratio without combination. However, as for the polyethylene/Cu coatings, a small diameter has more advantages for anti-combination, because the resistance originates from the hydrogen bubbles generated by electrochemical reactions. And P–Ni/Cu coatings show minimum tolerance of nearly 40% extrusion ratio without combination. Driven by 4 V electric or magnetic fields, LMs coated with polyethylene/Cu show reversible conductivity transformation and LMs coated with P–Ni/Cu show potential application in magnetic driven motions. Furthermore, this work presents an insightful way for the clustering and functional applications of LM based devices in solution.

Conflicts of interest

There are no conflicts to declare.

Acknowledgements

We thank the Yantai Double Hundred Talent Plan 2019, Science and Technology Support Plan for Youth Innovation of Colleges and Universities of Shandong Province of China (Grant No. 2021KJ089), Shandong Provincial Natural Science Foundation, (Grant No. ZR2020ME005, ZR2022ME197), Yantai science and technology innovation development plan, (Grant No.2022YT06810644), Doctoral Fund of Yantai Nanshan University, (Grant No. B202002, B202003, B202006, B202007, Q202020). And we also thank Xiaoyan Dong, Yantai Nanshan University, for the advice for this work.

Notes and references

1 T. Daeneke, K. Khoshmanesh, N. Mahmood, I. A. D. Castro, D. Esrafilzadeh, S. J. Barrow, M. D. Dickey and K. Kalantar-Zadeh, *Chem. Soc. Rev.*, 2018, **47**, 4073–4111.
2 K. Q. Ma and J. Liu, *J. Phys. D: Appl. Phys.*, 2007, **40**, 4722.
3 J. Guo, Y. Wang, X. Wang, Y. Xing and L. Hu, *Adv. Mater. Interfaces*, 2020, **7**, 2000732.
4 A. Chiolerio and M. B. Quadrelli, *Adv. Sci.*, 2017, **4**, 1700036.
5 L. Hu, L. Wang, Y. J. Ding, S. H. Zhan and J. Liu, *Adv. Mater.*, 2016, **28**, 9210–9217.
6 S. Cheeseman, A. Elbourne, S. Gangadoo, Z. L. Shaw, S. J. Bryant, N. Syed, M. D Dickey, M. J. Higgins, K. Vasilev, C. F McConville, A. J. Christofferson, R. J. Crawford, T. Daeneke, J. Chapman and V. K. Truong, *Adv. Mater. Interfaces*, 2022, **9**, 2102113.
7 S. Y. Tang, R. R. Qiao, S. Yan, D. Yuan, Q. B. Zhao, G. L. Yun, T. P. Davis and W. H. Li, *Small*, 2018, **14**, 1800118.
8 Y. Z. Chen, Z. Liu, D. Y. Zhu, S. H. Wang, S. Q. Liang, J. B. Yang, T. T. Kong, X. H. Zhou, Y. Z. Liu and X. C. Zhou, *Mater. Horiz.*, 2017, **4**, 591–597.
9 Y. Z. Chen, T. J. Zhou, Y. Y. Li, L. F. Zhu, S. H. Wang, D. Y. Zhu, X. H. Zhou, Z. Liu, T. S. Gan and X. C. Zhou, *Adv. Funct. Mater.*, 2018, **28**, 1706277.
10 J. L. Ma, H. X. Dong and Z. Z. He, *Mater. Horiz.*, 2018, **5**, 675–682.
11 N. Eustathopoulos, *Metals*, 2015, **5**, 350–370.
12 Z. Q. Gao, C. Dong, S. Y. Shang, M. L. Huang, H. T. Ma and Y. P. Wang, *Mater. Lett.*, 2021, **300**, 130137.
13 Y. T. Cui, F. Liang, Z. Yang, S. Xu, X. Zhao, Y. J. Ding, Z. S. Lin and J. Liu, *ACS Appl. Mater. Interfaces*, 2018, **10**, 9203–9210.
14 N. Zhang, P. Shen, Y. Cao, R. F. Guo and Q. C. Jiang, *Appl. Surf. Sci.*, 2019, **490**, 598–603.
15 J. B. Tang, X. Zhao, J. Li, Y. Zhou and J. Liu, *Adv. Sci.*, 2017, **4**, 1700024.
16 S. Chen, L. Wang, Q. Zhang and J. Liu, *Sci. Bull.*, 2018, **63**, 1513–1520.
17 R. C. Weas, *Handbook of Chemistry and Physics*, Wiley, Chichester, 70th edn, 1989, vol. D-151, pp. 121–125.
18 S. Y. Tang, K. Khoshmanesh, V. Sivan, P. Petersen, A. P. O'Mullane, D. Abbott, A. Mitchell and K. Kalantar-zadeh, *Proc. Natl. Acad. Sci. U. S. A.*, 2014, **111**, 3304–3309.
19 Md. A. Rahim, J. Tang, A. J. Christofferson, P. V. Kumar, N. Meftahi, F. Centurion, Z. Cao, J. Tang, M. Baharfar, M. Mayyas, F.-M. Allioux, P. Koshy, T. Daeneke, C. F. McConville, R. B. Kaner, S. P. Russo and K. Kalantar-Zadeh, *Nat. Chem.*, 2022, **14**, 935–941.
20 M. Mayyas, K. Khoshmanesh, P. Kumar, M. Mousavi, J. Tang, M. B. Ghasemian, J. Yang, Y. Wang, M. Baharfar, Md. A. Rahim, W. Xie, F.-M. Allioux, R. Daiyan, R. Jalili, D. Esrafilzadeh and K. Kalantar-Zadeh, *Adv. Func. Mater.*, 2022, **32**, 2108673.